Biochemistry

Article

pubs.acs.org/biochemistry

Rational Re-Engineering of the O-Dealkylation of 7-Alkoxycoumarin Derivatives by Cytochromes P450 2B from the Desert Woodrat *Neotoma lepida*

Lu Huo,[†,∥] Jingbao Liu,[†,⊥] M. Denise Dearing,[‡] Grazyna D. Szklarz,[§] James R. Halpert,[†] and P. Ross Wilderman*[,†]

[†]Department of Pharmaceutical Science, University of Connecticut School of Pharmacy, Storrs, Connecticut 06269-3092, United States

[‡]Department of Biology, University of Utah, Salt Lake City, Utah 84112, United States

[§]Department of Pharmaceutical Sciences, West Virginia University School of Pharmacy, Morgantown, West Virginia 26506, United States

Supporting Information

ABSTRACT: On the basis of recent functional and structural characterization of cytochromes P450 2B from the desert woodrat (*Neotoma lepida*), the 7-alkoxycoumarin and 7-alkoxy-4-(trifluoromethyl)coumarin O-dealkylation profiles of CYP2B35 and CYP2B37 were re-engineered. Point mutants interchanging residues at seven positions in the enzyme active sites were created and purified from an *Escherichia coli* expression system. In screens for O-dealkylation activity, wild-type CYP2B35 metabolized long-chain 7-alkoxycoumarins but not 7-alkoxy-4-(trifluoromethyl)coumarins or short-chain 7-alkoxycoumarins. Wild-type CYP2B37 metabolized short-chain substrates from both series of compounds. CYP2B35 A367V showed maximal activity with 7-butoxycoumarin as opposed to 7-heptoxycoumarin in the parental enzyme, and CYP2B35 A363I/A367V produced an activity profile like that generated by CYP2B37. CYP2B35 A363I/A367V/I477F showed 7-ethoxycoumarin and 7-ethoxy-4-(trifluoromethyl)coumarin O-dealkylation rates similar to those of CYP2B37 and higher than those of the double mutant. A CYP2B35 septuple mutant retained a CYP2B37-like activity profile. In contrast, the CYP2B37 septuple mutant produced very low rates of O-dealkylation of all substrates. As mutating residue 108 in either enzyme was detrimental, this change was removed from both septuple mutants. Remarkably, the CYP2B35 sextuple mutant produced an activity profile that was a hybrid of that of CYP2B35 and CYP2B37, whereas the CYP2B37 sextuple mutant had almost no O-dealkylation activity. Docking of 7-substituted coumarin derivatives into a model of the CYP2B35 sextuple mutant based on a previous crystal structure of the 4-(4-chlorophenyl)imidazole wild-type complex revealed how the mutant can exhibit activities of both CYP2B35 and CYP2B37.

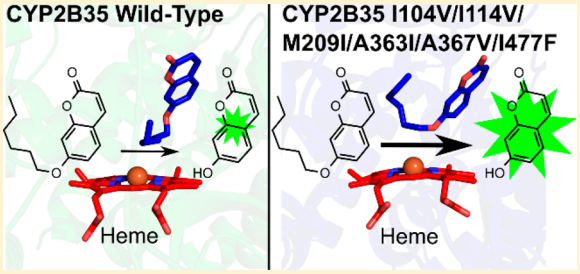

Cytochrome P450 (CYP)-dependent monooxygenases make up a superfamily of heme-containing enzymes that metabolize both endogenous and xenobiotic compounds.[1] Excretion or conjugation of hydrophobic compounds is facilitated by the insertion of molecular oxygen into hydrophobic substrates.[2] In mammals, CYP enzymes likely arose as a protective measure against the chemical diversity of toxic compounds produced by many plants.[3−5] Mammalian CYP enzymes involved in detoxification usually accept a broad array of compounds as substrates,[6,7] and the high degree of structural flexibility displayed by these enzymes likely contributes to their broad substrate specificity.[8−10] Investigations of CYP2B enzymes, which exhibit relatively low conservation of catalytic activity across mammalian species, have produced a substantial body of biochemical, biophysical, and structural information relating to protein−ligand and protein−protein interactions.[11]

Mammalian detoxification mechanisms in model organisms are well-documented; however, less attention has been paid to the contributions of CYP enzymes to the chemical ecology of wild mammalian species.[12,13] Plant secondary metabolites, compounds not essential for photosynthesis, may originally have been byproducts of primary metabolism and are involved in plant defense. Distinct populations of desert woodrats (*Neotoma lepida*) from the North American southwest are exposed to different toxins in their diets. Animals from the Great Basin consume large quantities of juniper (*Juniperus osteosperma*) in their diets, exposing them to high concentrations of terpenes and terpenoids, In contrast, the diet of animals from the Mojave Desert has a high percentage of creosote bush (*Larrea tridentata*), which likely displaced juniper in the Mojave Desert ∼18000 years ago as a result of natural

Received: February 6, 2017
Revised: March 29, 2017
Published: April 4, 2017

DOI: 10.1021/acs.biochem.7b00097
Biochemistry 2017, 56, 2238−2246

climate change; the resin of *L. tridentata* is composed mostly of phenolic compounds.[14]

Molecular characterization of enzymes involved in detoxification processes from wild populations is necessary for describing biotransformation mechanisms in wild herbivores, and current knowledge is gleaned from studies limited to a small subset of mammalian CYP enzymes involved in detoxification.[15−21] To address this gap, transcripts of CYP2B enzymes were previously isolated from *N. lepida* individuals that were captured either in the Great Basin Desert or in the Mojave Desert and fed either juniper or creosote bush in the laboratory.[22] Initial functional[23] and structural[24] characterization of CYP2B35[a] (representing transcripts from both populations regardless of diet), CYP2B36 (almost exclusively found in Great Basin woodrats fed juniper), and CYP2B37 (found only in Mojave Desert woodrats, regardless of diet) was previously performed in this laboratory. In screens of 7-alkoxycoumarin substrate O-dealkylation, CYP2B36 and CYP2B37 displayed the highest activities with 7-methoxy and 7-ethoxy derivatives containing a 4-(trifluoromethyl)coumarin core, respectively (Figure 1), and displayed a side-chain preference similar to those of rat CYP2B1, rabbit CYP2B4, and human CYP2B6.[25,26]

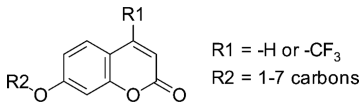

Figure 1. Chemical structure of 4-substitued 7-alkoxycoumarins.

In contrast, CYP2B35 displayed the greatest activity with 7-alkoxycoumarins with five to seven carbons in the alkoxy chain and little to no activity with substrates containing a 4-methylcoumarin or 4-(trifluoromethyl)coumarin core. Furthermore, the X-ray crystal structure of CYP2B35 [Protein Data Bank (PDB) entry 5E58] in complex with two molecules of 4-(4-chlorophenyl)imidazole (4-CPI)[24] highlighted the difference in active site volume between this enzyme (495 Å^3) and rabbit CYP2B4 (PDB entry 1SUO, 253 Å^3).[27] Furthermore, the X-ray crystal structures of rabbit CYP2B4 and human CYP2B6 (PDB entry 3IBD) contained only one molecule of 4-(4-chlorophenyl)imidazole in the active site.[28] The largest single contribution to this difference in coumarin derivative metabolism and active site topology is likely found at residues 363 and 367, where alanine is present at both positions in CYP2B35 versus isoleucine and valine in CYP2B4 and leucine and valine in CYP2B6, respectively (Table 1). Despite the differences in active site topology, the backbones of all three structures are virtually superimposable. In contrast, the CYP2B37−4-CPI complex was in a more open conformation, and three molecules of the inhibitor were observed in the structure, one in the active site and two within the substrate access channel.

Table 1. Amino Acid Identities of Residues 363 and 367 in CYP2B Enzymes

residue	2B1	2B2	2B4	2B5	2B6	2B11	2B35	2B37
363	V	A	I	V	L	L	A	I
367	V	L	V	A	V	V	A	V

Although X-ray crystal structures of CYP2B1, CYP2B11, CYP2B2, and CYP2B5 are not available, their amino acid sequences are known. CYP2B1 showed the highest activity for 7-methoxy- and 7-ethoxycoumarins when activity was screened using a series of 7-alkoxycoumarins.[25] CYP2B11 has a k_{cat} for 7-ethoxy-4-(trifluoromethyl)coumarin O-dealkylation [8.2 nmol min^{-1} (nmol of P450)$^{-1}$] similar to that of CYP2B4 [9.6 nmol min^{-1} (nmol of P450)$^{-1}$].[29,30] CYP2B2, with 95−96% amino acid identity to CYP2B1, displayed 1−3% of the 7-ethoxycoumarin O-dealkylation activity of CYP2B1,[31] and CYP2B5, possessing 97−98% amino acid identity to CYP2B4, displayed ∼35% of the 7-ethoxycoumarin O-dealkylation activity of CYP2B4.[32]

While CYP2B35 was isolated from animals from both the Great Basin and the Mojave Desert and CYP2B37 was isolated from only Mojave Desert animals, these two enzymes display ∼91% amino acid identity, with >40 differences across the entire sequence. However, only seven of these differences are found at positions previously identified as CYP2B active site residues, namely, I104V, I108F, I114V, M209I, A363I, A367V, and I477F (CYP2B35 amino acid, residue number, CYP2B37 amino acid). Previous successful rational re-engineering efforts using site-directed mutagenesis used more similar (CYP2B1 and CYP2B2[33] or CYP2B4 and CYP2B5[34]) or less similar (CYP2B1 and -2C9) enzymes.[35] With this in mind, we sought to explore the unusual substrate specificity of CYP2B35 in coumarin O-dealkylation by rationally re-engineering the coumarin substrate specificities of CYP2B35 and CYP2B37. Single and multiple mutants were tested with two series of 7-alkoxycoumarin derivatives with either a coumarin or a 4-(trifluoromethyl)coumarin core (Figure 1), leading to the discovery of a CYP2B35 mutant with activities of both parental enzymes.

EXPERIMENTAL PROCEDURES

Materials. CHAPS was purchased from EMD Chemicals (San Diego, CA). 5-Cyclohexyl-1-pentyl-β-D-maltoside (CYMAL-5) and isopropyl β-D-1-thiogalactopyranoside (IPTG) were obtained from Anatrace (Maumee, OH). Nickel-nitrilotriacetic acid (Ni^{2+}-NTA) affinity resin was purchased from Thermo Scientific (Rockford, IL). Macro-Prep CM cation exchange resin was received from Bio-Rad Laboratories (Hercules, CA). Amicon ultrafiltration devices were from Millipore (Billerica, MA). Plasmid pGro7 harboring the GroEL and GroES chaperones was from Takara Bio (Shiba, Japan). Arabinose, ampicillin, δ-aminolevulinic acid (ALA), chloramphenicol, phenylmethanesulfonyl fluoride (PMSF), lysozyme, dithiothreitol (DTT), 2-mercaptoethanol (β-ME), potassium phosphate, tryptone, and yeast extract required to prepare Luria-Bertani and Terrific broth media were purchased from Sigma-Aldrich. Sodium chloride (NaCl), ethylenediaminetetraacetic acid (EDTA), and glycerol were from Fisher Scientific, and L-histidine was from Spectrum Chemicals (New Brunswick, NJ).

7-Alkoxycoumarins were previously synthesized by E. Mash (Department of Chemistry, The University of Arizona, Tucson, AZ). 7-Hydroxy-4-(trifluoromethyl)coumarin (7-HFC) was purchased from Alfa Aesar (Ward Hill, MA). 7-Methoxy-4-(trifluoromethyl)coumarin (7-MFC) and 7-ethoxy-4-(trifluoromethyl)coumarin (7-EFC) were purchased from Life Technologies (Carlsbad, CA). The remaining 7-alkoxy-4-(trifluoromethyl)coumarins were previously synthesized by J. Liu.[24]

Site-Directed Mutagenesis. CYP2B35 and CYP2B37 single mutants were created using previously engineered

DOI: 10.1021/acs.biochem.7b00097
Biochemistry 2017, 56, 2238−2246

CYP2B35v1 and CYP2B37v2 genes as templates.[23] Single mutants were created followed by creation of constructs containing multiple mutations. Templates and primers used for construction of single and multiple mutants are listed in Table S1. All the mutants were generated by whole plasmid polymerase chain reaction using Phusion High-Fidelity DNA Polymerase (Thermo Scientific, Waltham, MA). Mutations were confirmed by sequencing at the University of Connecticut DNA Biotechnology Facility.

Protein Expression and Purification. CYP2B35dH, CYP2B37dH, or the respective mutant enzymes were expressed in OverExpress C43(DE3) chemically competent *E. coli* (Lucigen, Middleton, WI) containing the pGro7 plasmid that facilitates expression of the GroEL and GroES chaperone pair and purified using previously established methods.[36] Following expression, the harvested cell pellet was resuspended in 10% of the original culture volume in buffer containing 20 mM potassium phosphate (pH 7.4 at 4 °C), 20% (v/v) glycerol, 10 mM 2-mercaptoethanol (β-ME), and 1 mM phenylmethanesulfonyl fluoride (PMSF) and treated with 0.3 mg/mL lysozyme for 30 min while being stirred. The cells were then centrifuged for 30 min at 7500*g*. After the supernatant had been discarded, the spheroplasts were resuspended in 5% of the original culture volume in buffer containing 500 mM potassium phosphate (pH 7.4 at 4 °C), 20% (v/v) glycerol, 10 mM β-ME, 0.5 mM PMSF, and 10 mg/mL RNase A and DNase I and sonicated for 4 × 1 min on ice. CHAPS was added to the sample at a final concentration of 0.8% (w/v), and the solution was stirred for 90 min at 4 °C prior to ultracentrifugation for 1 h at 245000*g*. The CYP enzyme concentration was measured using the reduced carbon monoxide difference spectra.[37,38]

The supernatant was applied to a Ni^{2+}-NTA column. The column was washed with buffer containing 100 mM potassium phosphate (pH 7.4 at 4 °C), 100 mM NaCl, 20% (v/v) glycerol, 10 mM β-ME, 0.5 mM PMSF, 0.5% (w/v) CHAPS, and 5 mM histidine, and the protein was eluted using buffer containing 10 mM potassium phosphate (pH 7.4 at 4 °C), 100 mM NaCl, 20% (v/v) glycerol, 10 mM β-ME, 0.5 mM PMSF, 0.5% (w/v) CHAPS, and 50 mM histidine. Protein quality was measured by the A_{417}/A_{280} ratio, and the highest-quality protein was collected. Following measurement of the CYP enzyme concentration using the reduced carbon monoxide difference spectra, the sample was diluted at least 10-fold with buffer containing 5 mM potassium phosphate (pH 7.4 at 4 °C), 20% (v/v) glycerol, 1 mM EDTA, 0.2 mM dithiothreitol (DTT), 0.5 mM PMSF, and 0.5% (w/v) CHAPS followed by loading onto a Macro-Prep CM column. The CM column was washed using low-salt buffer containing 5 mM potassium phosphate (pH 7.4 at 4 °C), 20% (v/v) glycerol, 1 mM EDTA, and 0.2 mM DTT. The protein was eluted with high-salt buffer containing 50 mM potassium phosphate (pH 7.4 at 4 °C), 500 mM NaCl, 20% (v/v) glycerol, 1 mM EDTA, and 0.2 mM DTT. The quality of protein fractions was measured using the A_{417}/A_{280} ratio, and the highest-quality CYP enzyme fractions were pooled. The CYP enzyme concentration was measured using the reduced carbon monoxide difference spectra followed by dialysis against buffer containing 20 mM potassium phosphate (pH 7.4 at 4 °C) and 20% (v/v) glycerol.

Enzymatic Assays. The rate of O-dealkylation of 7-alkoxycoumarins (7-AC) and 7-alkoxy-4-(trifluoromethyl)-coumarins (7-AFC) was measured as described previously.[23,39] Each series of 7-alkoxycoumarin derivatives contained samples with a range of one to seven carbons in the alkoxy chain. The reconstituted enzyme system contained cytochrome P450, rat NADPH-cytochrome P450 reductase,[40] and rat cytochrome b_5[41] at a molar ratio of 1:4:2. Reconstitution of these enzymes was performed by addition to 20 mM potassium phosphate (pH 7.4) and 20% glycerol (v/v) in a final volume of 10 μL in the following order with gentle mixing using a pipet: (1) NADPH-cytochrome P450 reductase, (2) cytochrome b_5, and (3) cytochrome P450. Reactions were performed in a 100 μL final volume containing 50 mM HEPES (pH 7.4) and 15 mM $MgCl_2$ with a final CYP enzyme concentration of 0.1 μM. The substrate concentration was 200 μM for substrate preference profile determination and 0−200 μM for steady-state kinetic assays. The 3 min preincubation and enzymatic reactions were performed at 37 °C and initiated by addition of NADPH to a final concentration of 1 mM.

In screening assays using 7-alkoxycoumarin substrates, the reactions were quenched after 10 min by the addition of 25 μL of 2 M HCl. The quenched reaction mixture was extracted with 450 μL of chloroform and centrifuged at 3000*g* for 5 min. A 1.0 mL aliquot of a 30 mM sodium borate solution (pH 9.2) was used to extract the O-dealkylation product, 7-hydroxycoumarin, from 300 μL of the chloroform phase. This mixture was centrifuged at 3000*g* for 5 min, and a 900 μL aliquot of the aqueous phase was removed for analysis. The fluorescence of the product in the borate solution was determined using a Hitachi F2000 fluorescence spectrophotometer (Hitachi, Tokyo, Japan) using a λ_{ex} of 370 nm and a λ_{em} of 450 nm for 7-hydroxycoumarin. Product formation by CYP2B35 or CYP2B35 SxM in O-dealkylation assays using 7-alkoxycoumarins was linear up to 20 min. In screening assays using 7-alkoxy-4-(trifluoromethyl)coumarin substrates, reactions were quenched by addition of 50 μL of ice-cold acetonitrile after 10 min. A 50 μL aliquot of the quenched solution was then transferred to a tube containing 950 μL of 0.1 M Tris (pH 9.0). The fluorescence of the product, 7-hydroxy-4-(trifluoromethyl)coumarin, was determined using a Hitachi F2000 fluorescence spectrophotometer using a λ_{ex} of 410 nm and a λ_{em} of 510 nm. Calibration was performed on the same day by measuring the fluorescence intensity of synthesized products at concentrations of 0.5−2 μM under the same conditions. Data were fit to the Michaelis−Menten or substrate inhibition equation using Origin (OriginLab, Northhampton, MA) or Igor Pro 7.0 (Wavemetrics, Inc., Portland, OR).

Molecular Modeling Simulations. All molecular modeling was performed on an SGI Octane workstation with the Insight II/Discover software package (Accelrys, Inc., San Diego, CA) using a consistent valence force field supplemented with parameters for heme.[42,43] Alkoxycoumarin substrates, including 7-ethoxycoumarin, 7-butoxycoumarin, 7-hexoxycoumarin, 7-heptoxycoumarin, and 7-ethoxy-4-(trifluoromethyl)coumarin, were built and energy optimized using the Builder module of InsightII. The X-ray crystal structures of CYP2B35 and CYP2B37 were prepared previously, as described by Shah and co-workers.[24] To prepare the CYP2B35 mutant containing six residue substitutions, I104V, I114V, M209I, A363I, A367V, and I477F, mutated residues were replaced with the appropriate amino acids using the Biopolymer module of InsightII. The region containing the mutations was then subjected to structural refinement using a combination of minimization and molecular dynamics. Initially, the geometric center of the region was identified using a pseudoatom, and a sphere with a radius of 10 Å was defined. The atoms contained in that sphere were allowed to move, while the rest of the molecule was kept

DOI: 10.1021/acs.biochem.7b00097
Biochemistry 2017, 56, 2238−2246

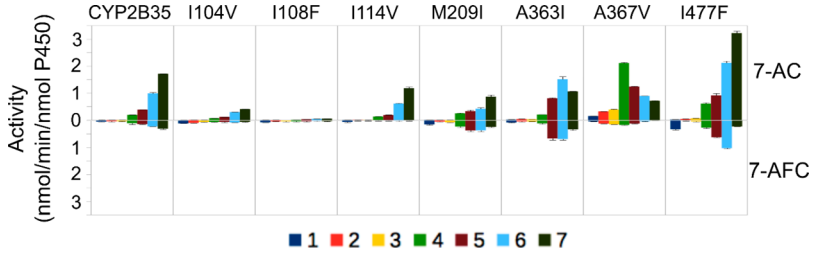

Figure 2. 7-Alkoxycoumarin and 7-alkoxy-4-(trifluoromethyl)coumarin O-dealkylation profiles of CYP2B35 single mutants. The activity was measured at 200 μM substrate as described in Experimental Procedures. The bars represent the means obtained from three independent determinations ± the 95% confidence limit. 7-AC denotes 7-alkoxycoumarin and 7-AFC 7-alkoxy-4-(trifluoromethyl)coumarin. The legend represents the number of carbons in the 7-alkoxy chain.

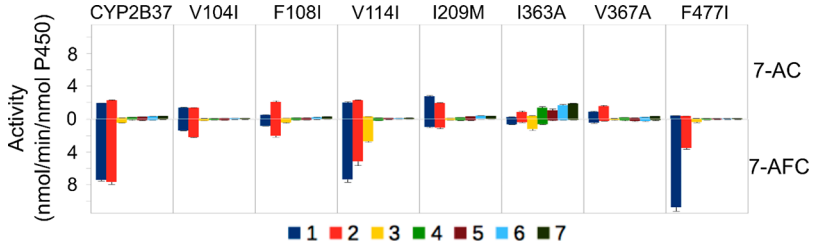

Figure 3. 7-Alkoxycoumarin and 7-alkoxy-4-(trifluoromethyl)coumarin O-dealkylation profiles of CYP2B37 single mutants. The activity was measured at 200 μM substrate as described in Experimental Procedures. The bars represent the means obtained from three independent determinations ± the 95% confidence limit. 7-AC denotes 7-alkoxycoumarin and 7-AFC 7-alkoxy-4-(trifluoromethyl)coumarin. The legend represents the number of carbons in the 7-alkoxy chain.

fixed. The refinement protocol involved 1000 steps of steepest descent minimization in vacuo using a distance-dependent dielectric, followed by 1 ps molecular dynamics at 300 K, and again by minimization under the same conditions, as described previously.[44] The ligands were initially placed manually into the active site of the enzymes in binding orientations consistent with O-dealkylation using the Docking module of InsightII, as described previously.[44−46] To determine the optimal ligand conformation, a dynamic docking approach was used, in which the substrate and the enzyme residues within 5 Å of the substrate were allowed to move, and a 5 Å distance restraint was imposed between the heme iron and the carbon of the substrate at which oxidation would take place. The enzyme−substrate complex was subjected to 1000 steps of minimization using steepest descent followed by 1 ps molecular dynamics simulations at 300 K.[47,48] The resulting trajectory was analyzed to find the best substrate orientation, and the enzyme−substrate complex was minimized for another 1000 steps, as described above. This optimal substrate orientation was used as a starting point for docking with the Affinity module of Insight II, as described previously.[49−52] Twenty distinct binding complexes obtained by the Monte Carlo search technique were subjected to simulated annealing prior to energy ranking, and the 10 lowest-energy binding orientations were selected for further analysis. The most energetically favorable enzyme−ligand complex was chosen to represent the binding orientation of the substrate, and a productive orientation was defined as a pose in which the distance between the heme iron and the carbon at the oxidation site was <5−6 Å.

RESULTS

CYP2B35 M209I, A363I, A367V, and I477F Show Altered 7-AC or 7-AFC O-Dealkylation Activity. Mutants were constructed at the seven active site positions where CYP2B35 and CYP2B37 differ, and O-dealkylation was assessed using two series of 4-substituted 7-ACs. As previously seen, wild-type CYP2B35 had the highest activity with 7-heptoxycoumarin followed by 7-hexoxycoumarin and 7-pentoxycoumarin in decreasing order and did not efficiently dealkylate substrates containing the 4-(trifluoromethyl)-coumarin core (Figure 2 and Tables S2 and S3).[24] Using 7-AC substrates at 200 μM, A363I displayed its greatest activity with 7-hexoxycoumarin, and A367V exhibited its greatest activity with 7-butoxycoumarin. I104V, I114V, M209I, and I477F showed unaltered chain-length preference. Relative to that of wild-type CYP2B35, I477F exhibited increased O-dealkylation rates of substrates containing four to seven carbons in the alkoxy chain. In contrast, screening for activity using 7-AFCs showed increases relative to those of wild-type CYP2B35 with M209I, A363I, and I477F.

CYP2B37 I363A and F477I Show Altered Activity Using 7-AC Substrates. In contrast to CYP2B35, wild-type CYP2B37 readily dealkylates substrates containing shorter alkoxy chains and has greater activity with 7-AFCs than with 7-ACs (Figure 3 and Tables S4 and S5). With 7-AFCs, F108I showed a >2-fold change in the ratio of 7-methoxy-4-(trifluoromethyl)coumarin to 7-ethoxy-4-(trifluoromethyl)-coumarin O-dealkylation and F108I and V367A showed an altered ratio of activity with 7-methoxycoumarin versus 7-ethoxycoumarin. In neither series was an increased level of O-dealkylation of longer-chain compounds observed with F108I or V367A. CYP2B37 V114I and I363A exhibited increased levels of O-dealkylation of 7-propoxy-4-(trifluoromethyl)-coumarin. V367A had decreased activity with all 7-AFC substrates. I363A showed increased O-dealkylation activity with 7-AC substrates containing four to seven carbons in the alkoxy chain and decreased activity with shorter alkoxy-chain 7-AC substrates.

Combining Mutations Produced Different Results in CYP2B35 and CYP2B37. With the idea of altering the ability

DOI: 10.1021/acs.biochem.7b00097
Biochemistry 2017, 56, 2238−2246

of CYP2B35 and CYP2B37 to dealkylate 7-EFC and 7-heptoxycoumarin, respectively, combinations of mutations at residues 363, 367, and 477 were created. As expected, CYP2B35 A363I/A367V showed significant O-dealkylation activity with 7-methoxycoumarin and 7-ethoxycoumarin, very low O-dealkylation activity with 7-AC derivatives containing four to seven carbons, and low O-dealkylation activity with 7-EFC (Figure 4A and Tables S2 and S3). Addition of the I477F

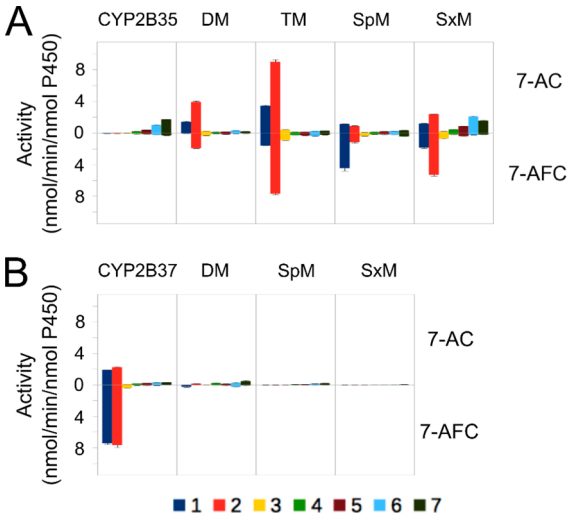

Figure 4. 7-Alkoxycoumarin and 7-alkoxy-4-(trifluoromethyl)-coumarin O-dealkylation profiles of various multiple mutants of CYP2B35 and CYP2B37. The mutants of (A) CYP2B35 and (B) CYP2B37 were screened using 7-AC and 7-AFC substrate series. The activity was measured using 200 μM substrate, as described in Experimental Procedures. The bars represent the means obtained from three independent determinations ± the 95% confidence limit. 7-AC denotes 7-alkoxycoumarin, 7-AFC 7-alkoxy-4-(trifluoromethyl)-coumarin, DM the double mutant at residues 363 and 367, TM the triple mutant at residues 363, 367, and 477, SpM the septuple mutant combining all seven single mutations, and SxM the sextuple mutant in which the mutation at residue 108 was removed. The legend represents the number of carbons in the 7-alkoxy chain.

substitution to CYP2B35 A363I/A367V increased activity toward substrates having one or two carbons in the alkoxy chain but little or no change in activity with coumarin derivatives containing four to seven carbon alkoxy chains. In contrast to CYP2B35 mutants, combinations of mutations in CYP2B37 resulted in loss of 7-AC and 7-AFC O-dealkylation activity (Figure 4B and Tables S4 and S5). Addition of I104V, I108F, I114V, and M209I to CYP2B35 A363I/A367V/I477F decreased activity significantly with all C1−C3 substrates except 7-methoxy-4-(trifluoromethyl)coumarin. Because mutating residue 108 alone caused almost total loss of O-dealkylation activity in CYP2B35 without selecting for a CYP2B37-like O-dealkylation profile, F108 was mutated back to Ile in the CYP2B35 septuple mutant (SpM), generating the I104V/I114V/M209I/A363I/A367V/I477F sextuple mutant (SxM). Surprisingly, the CYP2B35 SxM retained O-dealkylation activity with short-chain coumarin substrates in both series combined with higher activity toward longer-chain 7-AC derivatives, thus resulting in a profile that was a hybrid of those of CYP2B35 and CYP2B37.

Steady-State Kinetic Analysis of CYP2B35 and CYP2B35 SxM Using 7-EC, BuC, and HxC. With each substrate, CYP2B35 SxM had a catalytic efficiency of O-dealkylation higher than that of wild-type CYP2B35 (Table 2). With 7-EC, CYP2B35 SxM gained O-deethylation activity. With 7-BuC and 7-HxC, the increased catalytic efficiency of CYP2B35 SxM metabolism compared to that of the wild-type enzyme is mostly due to a higher affinity for the substrate. Furthermore, wild-type CYP2B35 exhibited substrate inhibition with these two substrates, whereas CYP2B35 SxM did not.

Docking of 7-Alkoxycoumarin Derivatives into the Active Sites of Wild-Type CYP2B35 and Its Sextuple Mutant. To explain the drastically altered product profile obtained with alkoxycoumarin substrates for the CYP2B35 SxM compared to that of wild-type CYP2B35, molecular modeling was used. 7-MC, 7-EC, and 7-EFC were docked into the model of the CYP2B35 SxM, and 7-BuC and 7-HxC were docked into models of both wild-type CYP2B35 and the SxM. Previous results indicated that 7-EC and 7-EFC do not yield binding poses conducive to O-dealkylation when docked into wild-type CYP2B35.[24] In contrast, of the 10 lowest-energy poses obtained from docking 7-EC into CYP2B35 SxM (198−213 kcal/mol), four were conducive to O-dealkylation (Figure 5A). Likewise, docking of 7-EFC into CYP2B35 SxM produced a similar energy range for the 10 lowest-energy poses (134−149 kcal/mol) with half of the poses likely to lead to O-dealkylation (Figure 5B). Interestingly, similar results were obtained for 7-MC docked into CYP2B35 SxM, yielding 4 of the 10 lowest-energy poses (122−142 kcal/mol) consistent with O-demethylation (not shown), while in the case of wild-type

Table 2. Steady-State Kinetics of Substrate Oxidation by Wild-Type (wt) CYP2B35 and Its Sextuple Mutant

		7-alkoxycoumarin O-dealkylation		
substrate	enzyme	k_{cat} [a]	K_M (μM)	k_{cat}/K_M [b]
7-EC	CYP2B35 wt	ND[c]		
	CYP2B35 SxM	3.0 ± 0.2	41.4 ± 12.0	0.072 ± 0.022
7-BuC	CYP2B35 wt	0.8 ± 0.2	177.3 ± 55.4	0.005 ± 0.002
			K_I = 75.6 ± 24.7 μM	
	CYP2B35 SxM	0.6 ± 0.1	45.7 ± 7.7	0.013 ± 0.003
7-HxC	CYP2B35 wt	3.6 ± 0.8	69.6 ± 24.0	0.052 ± 0.021
			K_I = 103.5 ± 35.1 μM	
	CYP2B35 SxM	2.8 ± 0.2	12.6 ± 4.2	0.222 ± 0.076

[a]Reported as nanomoles of product per minute per nanomole of P450. [b]Reported as nanomoles of product per minute per nanomole of P450 per micromolar. [c]Results are the average ± standard deviation of three or four independent experiments performed in duplicate. ND, not detectable above background. The maximal fluorescence was less than twice the zero product value, corresponding to 7-HC production rates below ~0.05 nmol min^{-1} (nmol of P450)$^{-1}$.

DOI: 10.1021/acs.biochem.7b00097
Biochemistry 2017, 56, 2238−2246

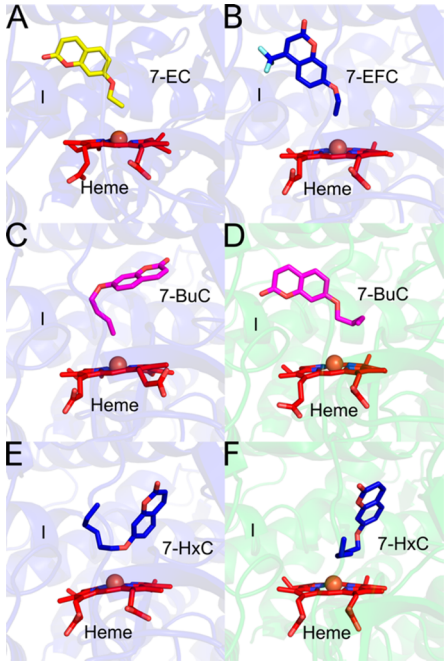

Figure 5. 7-Alkoxycoumarin derivatives docked into the wild-type CYP2B35 crystal structure and a model of the CYP2B35 SxM. Representative poses conducive to O-dealkylation are shown. The heme is shown as red sticks, and the heme iron is shown as a brick red sphere. Docking of (A) 7-EC and (B) 7-EFC into the active site of CYP2B35 SxM revealed poses likely to facilitate O-dealkylation. Docking runs using 7-BuC revealed fewer poses consistent with O-dealkylation in both the (C) CYP2B35 SxM and (D) wild-type enzymes than docking 7-HxC in (E) CYP2B35 SxM and (F) wild-type enzymes.

CYP2B35, none of the 10 poses (94−119 kcal/mol) led to substrate oxidation, which agrees with experimental data. Consistent with the lower activity in screening assays with 7-BuC, the highest-affinity poses from simulations using CYP2B35 SxM or wild-type CYP2B35 (not shown) were oriented so that the site of metabolism was more than 5−6 Å from the heme iron, oriented away from the heme, or both; fewer poses represented orientations likely to lead to O-dealkylation by either the CYP2B35 SxM (2 of 10 poses) or wild-type CYP2B35 (1 pose) (Figure 5C,D). Of the 10 lowest-energy poses for 7-HxC docked into the CYP2B35 SxM or wild-type CYP2B35, three poses were likely to lead to O-dealkylation (Figure 5E,F).

DISCUSSION

Most available information about ligand interactions with CYP enzymes is in the context of drug metabolism by humans and laboratory animals. The xenobiotic metabolizing CYP enzymes are thought to have evolved in response to challenge by dietary toxins;[53] however, rigorous biochemical studies of CYP enzymes in species that regularly encounter dietary toxins in nature are sparse. Recent functional and structural characterization of CYP enzymes from the desert woodrat (*N. lepida*), a mammalian herbivore that ingests high levels of toxins in its natural diet, revealed differences in the abilities of CYP2B35 and CYP2B37 to metabolize model substrates that are related to differences in the size of the enzyme active sites.[23,24] However, most of the >40 residue differences between the enzymes lie outside of the active site, and considerable evidence from multiple CYP enzymes indicates the importance of non-active site residues for enzyme function.[30,54−56] This investigation revealed that interconverting a small number of amino acid residues in the active site of these enzymes shifted the substrate preference toward the other enzyme's profile; furthermore, the effects of multiple mutations were not necessarily predicted from the profiles of the individual mutants involved.

As seen in previous work that examined determinants of regio- and stereoselectivity of androstenedione hydroxylation by CYP2B4 and CYP2B5[34] and conferred the progesterone hydroxylase activity of CYP2C5 onto CYP2B1,[35] a small set of mutants shifted the product profile of the modified enzyme in the desired direction. In each case, conversion of residue 363, residue 367, or both produced a significant change in product outcome. Changes in the amino acid side-chain bulk at these residues changed the space available for substrates near the active oxoferryl iron (Compound I). In contrast, previous mutants of residue 114 in CYP2B1 or CYP2B5 led to changes in the product profile larger than mutation of this residue in CYP2B35 or CYP2B37. This difference in the magnitude of the functional changes could be due to the relative change in the bulk of the amino acid introduced into the active site. Conversion of CYP2B1 Ile-114 to Ala, which increased progesterone hydroxylation activity, removed both γ-carbons in addition to the δ-carbon, and replacing CYP2B5 Phe-114 with Ile, which decreased progesterone hydroxylation activity, removed a rigid ring from the active site. In contrast, the smaller change in side-chain volume and the ability of the Ile δ-carbon to rotate relative to the bond between the β-carbon and the γ-carbon in CYP2B35 I114V and CYP2B37 V114I likely led to a relatively small change in the effective volume and ensuing small changes in screening profiles relative to those of the respective wild-type enzymes.

While the shift in metabolism by CYP2B35 A363I/A367V is noteworthy, the lack of O-dealkylation products for any tested combination of mutants in CYP2B37 is also extraordinary. A clue about this result may be found in the relative orientations of 7-EFC when docked into the CYP2B35 and CYP2B37 models based on crystal structures (Figure 5E,F of ref 23). With the extra space near the heme in CYP2B37 I363A/V367A, 7-AC substrates may not have the alkoxy oxygen sufficiently close to the heme for bond cleavage, and 7-AFC substrates may reorient with the 4-(trifluoromethyl)coumarin ring system toward the heme instead of the 7-alkoxy moiety, leading to a lack of O-dealkylation activities.

The most striking observation was the functional properties obtained with the CYP2B35 SxM. This combination of mutations confers a dealkylation activity profile intermediate between that of CYP2B35 and CYP2B37, namely, greater activity with longer alkoxy-chain 7-ACs but lower activity with longer-chain 7-AFCs and high activity with shorter-chain 7-ACs and 7-AFCs. A similar gain of function without loss of parental function was seen with androstenedione and testosterone hydroxylation by CYP2B1 F206L.[33] Wild-type CYP2B1 has 16β-, 16α-, and 15α-hydroxylase activities (D-ring); CYP2B1 F206L retained the hydroxylation activity on the D-ring in addition to gaining androstenedione and testosterone 6α-hydroxylase and 7α-testosterone hydroxylase activity (B-ring).[33] Restrained molecular docking of 7-EC, 7-EFC, 7-BuC, and 7-HxC into CYP2B35 and the CYP2B35 SxM indicated that only 7-HxC is oriented properly for O-dealkylation in CYP2B35, while 7-EC, 7-EFC, and 7-HxC are

DOI: 10.1021/acs.biochem.7b00097
Biochemistry 2017, 56, 2238−2246

positioned correctly in CYP2B35 SxM. Previous molecular docking experiments involving CYP2B35 revealed that 7-HpC was oriented properly for O-dealkylation. Thus, because both 7-HxC and 7-HpC are O-dealkylated by CYP2B35 and the CYP2B35 SxM, 7-HpC must orient properly for metabolism in the CYP2B35 SxM active site, but 7-HpC was not docked into the CYP2B35 SxM.

In our mutagenesis studies, the most critical determinants of enzyme−ligand interactions are residues from the previously identified SRS regions: 104, 108, and 114 (SRS-1), 206 and 209 (SRS-2), 294 and 302 (SRS-4), 363 and 367 (SRS-5), and 477 and 478 (SRS-6). However, no trend was previously seen between the effect of altering the bulk of the amino acid side chain and the specific SRS where the residue was located. In contrast with CYP2B35 and CYP2B37, changes in bulk due to mutations in SRS-1 decreased dealkylation activity compared with that of the wild-type enzyme, especially at residue 108; this result could be due to reorientation of the preferred pose of the coumarin rings as depicted in panels A and B of Figure 5, as well as Figure 5 of ref 23. Mutations leading to changes in the bulk of active site amino acids in SRS-5 had the greatest effect on altering the alkoxy chain-length preference. Changes in bulk to active site residues in SRS-6 increased dealkylation activity for substrates preferred by the wild-type enzyme. Previous investigations of determinants of CYP2B−ligand interactions noted that decreased side-chain bulk at residues 114, 206, 363, and 367 allowed for 6β- or 21-hydroxylation of progesterone by CYP2B1.[33,35] A decrease in side-chain bulk at residues 114, 206, 302, 363, and 478 in CYP2B1 also led to a decrease in β-OH:α-OH ratios for androstenedione and testosterone hydroxylation, but this ratio increased with decreased side-chain bulk at residue 367.

It is possible that the differences observed in CYP2B35 and CYP2B37 in the dealkylation of coumarin derivatives provide a physiological advantage to those *N. lepida* individuals that possess copies of both CYP2B isoforms. The individuals documented to possess both isozymes are restricted to a population that feeds on creosote bush (*L. tridentata*), an extremely toxic shrub of the U.S. desert southwest.[22] Creosote bush invests heavily in a battery of defensive compounds, with up to 20% of its dry matter committed to a resin containing more than 300 natural products that include highly bioactive lignans, flavonoids, saponins, and terpenes.[57,58] It is possible that CYP2B37 metabolizes some of these novel compounds that are not found in the diets of *N. lepida* that do not feed on creosote. In total, the increased space seen in the active site of CYP2B35 likely allows alternate substrate binding orientations and a unique coumarin substrate specificity among CYP2B enzymes. The preference profiles obtained in this study provide insights into the contribution of active site residue identity and substrate size on CYP2B catalysis. Further studies using solution biophysical methods, monitoring of alternate product formation, and other substrates, specific for both CYP2B and non-CYP2B, will improve our understanding of the determinants of substrate recognition in CYP2B enzymes and other xenobiotic metabolizing CYP enzymes.

■ ASSOCIATED CONTENT

Supporting Information

The Supporting Information is available free of charge on the ACS Publications website at DOI: 10.1021/acs.biochem.7b00097.

Tables showing the primers used for site-directed mutagenesis and O-dealkylation rates from screening assays and a figure displaying the amino acid residues that are different in the active sites of CYP2B35 and CYP2B37 (PDF)

■ AUTHOR INFORMATION

Corresponding Author

*E-mail: ross.wilderman@uconn.edu.

ORCID

P. Ross Wilderman: 0000-0002-0264-1704

Present Addresses

[‖]L.H.: Alliance Pharma, Malvern, PA 19355.

[⊥]J.L.: Department of Pharmaceutical Chemistry, University of California, San Francisco, School of Pharmacy, San Francisco, CA 94158.

Funding

This research was supported by National Science Foundation Grant IOS 1256840 to J.R.H.

Notes

The authors declare no competing financial interest.

■ ABBREVIATIONS

CYP, cytochrome P450-dependent monooxygenase; 7-AC, 7-alkoxycoumarin; 7-AFC, 7-alkoxy-4-(trifluoromethyl)coumarin; CHAPS, 3-[(3-cholamidopropyl)dimethylammonia]-1-propanesulfonate; CYMAL-5, 5-cyclohexyl-1-pentyl-β-D-maltoside; IPTG, isopropyl β-D-1-thiogalactopyranoside; Ni^{2+}-NTA, nickel-nitrilotriacetic acid; ALA, δ-aminolevulinic acid; PMSF, phenylmethanesulfonyl fluoride; DTT, dithiothreitol; β-ME, 2-mercaptoethanol; NaCl, sodium chloride; EDTA, ethylenediaminetetraacetic acid; 7-HFC, 7-hydroxy-4-(trifluoromethyl)coumarin; 7-HMC, 7-hydroxy-4-methylcoumarin; 7-MFC, 7-methoxy-4-(trifluoromethyl)coumarin; 7-EFC, 7-ethoxy-4-(trifluoromethyl)coumarin; CYP2B35 SpM, CYP2B35 septuple mutant (I104V/I108F/I114V/M209I/A363I/A367V/I477F); CYP2B35 SxM, CYP2B35 sextuple mutant (I104V/I114V/M209I/A363I/A367V/I477F); CYP2B37 SpM, CYP2B37 septuple mutant (V104I/F108I/V114I/I209M/I363A/V367A/F477I); CYP2B37 SxM, CYP2B37 sextuple mutant (V104I/V114I/I209M/I363A/V367A/F477I).

■ ADDITIONAL NOTE

[a]In this work, CYP2B35 and CYP2B37 refer to CYP2B35v1dH and CYP2B37v2dH, respectively, unless otherwise stated. These enzymes are N-terminally truncated and engineered and C-terminally His-tagged forms of CYP2B35v1 and CYP2B37v2, respectively.

■ REFERENCES

(1) Johnson, E. F., and Stout, C. D. (2013) Structural Diversity of Eukaryotic Membrane Cytochrome P450s. *J. Biol. Chem. 288*, 17082−17090.

(2) Guengerich, F. P., and Isin, E. M. (2008) Mechanisms of cytochrome P450 reactions. *Acta Chim. Slov. 55*, 7−19.

(3) Gonzalez, F. J. (1988) The Molecular-Biology of Cytochrome P450s. *Pharmacol. Rev. 40*, 243−288.

(4) Stamp, N. (2003) Out of the quagmire of plant defense hypotheses. *Q. Rev. Biol. 78*, 23−55.

(5) Weng, J.-K., Philippe, R. N., and Noel, J. P. (2012) The Rise of Chemodiversity in Plants. *Science 336*, 1667−1670.

DOI: 10.1021/acs.biochem.7b00097
Biochemistry 2017, 56, 2238−2246

(6) Anzenbacher, P., Anzenbacherova, E., Lange, R., Skopalik, J., and Otyepka, M. (2008) Active sites of cytochromes P450: What are they like? *Acta Chim. Slov. 55*, 63−66.
(7) Poulos, T. L. (2005) Structural and functional diversity in heme monooxygenases. *Drug Metab. Dispos. 33*, 10−18.
(8) Otyepka, M., Berka, K., and Anzenbacher, P. (2012) Is there a relationship between the substrate preferences and structural flexibility of cytochromes P450? *Curr. Drug Metab. 13*, 130−142.
(9) Poulos, T. L. (2005) Structural biology of heme monooxygenases. *Biochem. Biophys. Res. Commun. 338*, 337−345.
(10) Wilderman, P. R., and Halpert, J. R. (2012) Plasticity of CYP2B enzymes: structural and solution biophysical methods. *Curr. Drug Metab. 13*, 167−176.
(11) Zhao, Y., and Halpert, J. R. (2007) Structure-function analysis of cytochromes P450 2B. *Biochim. Biophys. Acta, Gen. Subj. 1770*, 402−412.
(12) Al Omari, A., and Murry, D. J. (2007) Pharmacogenetics of the cytochrome P450 enzyme system: Review of current knowledge and clinical significance. *Journal of Pharmacy Practice 20*, 206−218.
(13) Dearing, M. D., Foley, W. J., and McLean, S. (2005) The influence of plant secondary metabolites on the nutritional ecology of herbivorous terrestrial vertebrates. *Annu. Rev. Ecol. Evol. Syst. 36*, 169−189.
(14) Hunter, K. L., Betancourt, J. L., Riddle, B. R., Van Devender, T. R., Cole, K. L., and Spaulding, W. G. (2001) Ploidy race distributions since the Last Glacial Maximum in the North American desert shrub. *Larrea tridentata 10*, 521−533.
(15) El-Merhibi, A., Ngo, S., Jones, B., Milic, N., Stupans, I., and Mckinnon, R. (2008) Molecular insights into xenobiotic disposition in Australian Marsupials. *Australas. J. Ecotoxicol. 13*, 53−64.
(16) El-Merhibi, A., Ngo, S. N. T., Crittenden, T. A., Marchant, C. L., Stupans, I., and McKinnon, R. A. (2011) Cytochrome P450 CYP3A in marsupials: Cloning and characterisation of the second identified CYP3A subfamily member, isoform 3A78 from koala (Phascolarctos cinereus). *Comp. Biochem. Physiol., Part C: Toxicol. Pharmacol. 154*, 367−376.
(17) El-Merhibi, A., Ngo, S. N. T., Marchant, C. L., Height, T. A., Stupans, I., and McKinnon, R. A. (2012) Cytochrome P450 CYP3A in marsupials: Cloning and identification of the first CYP3A subfamily member, isoform 3A70 from Eastern gray kangaroo (Macropus giganteus). *Gene 506*, 423−428.
(18) Haley, S. L., Lamb, J. G., Franklin, M. R., Constance, J. E., and Dearing, M. D. (2007) Xenobiotic metabolism of plant secondary compounds in oak (*Quercus agrifolia*) by specialist and generalist woodrat herbivores, genus *Neotoma*. *J. Chem. Ecol. 33*, 2111−2122.
(19) Haley, S. L., Lamb, J. G., Franklin, M. R., Constance, J. E., and Denise Dearing (2007) Xenobiotic metabolism of plant secondary compounds in juniper (*Juniperus monosperma*) by specialist and generalist woodrat herbivores, genus Neotoma. *Comp. Biochem. Physiol., Part C: Toxicol. Pharmacol. 146*, 552−560.
(20) Magnanou, E., Malenke, J. R., and Dearing, M. D. (2009) Expression of biotransformation genes in woodrat (Neotoma) herbivores on novel and ancestral diets: identification of candidate genes responsible for dietary shifts. *Mol. Ecol. 18*, 2401−2414.
(21) Skopec, M. M., Haley, S., and Dearing, M. D. (2007) Differential hepatic gene expression of a dietary specialist (Neotoma stephensi) and generalist (Neotoma albigula) in response to juniper (Juniperus monosperma) ingestion. *Comp. Biochem. Physiol., Part D: Genomics Proteomics 2*, 34−43.
(22) Malenke, J. R., Magnanou, E., Thomas, K., and Dearing, M. D. (2012) Cytochrome P450 2B Diversity and Dietary Novelty in the Herbivorous, Desert Woodrat (*Neotoma lepida*). *PLoS One 7*, e41510.
(23) Wilderman, P. R., Jang, H. H., Malenke, J. R., Salib, M., Angermeier, E., Lamime, S., Dearing, M. D., and Halpert, J. R. (2014) Functional characterization of cytochromes P450 2B from the desert woodrat Neotoma lepida. *Toxicol. Appl. Pharmacol. 274*, 393−401.
(24) Shah, M. B., Liu, J., Huo, L., Zhang, Q., Dearing, M. D., Wilderman, P. R., Szklarz, G. D., Stout, C. D., and Halpert, J. R. (2016) Structure-function analysis of mammalian CYP2B enzymes using 7-substituted coumarin derivatives as probes: utility of crystal structures and molecular modeling in understanding xenobiotic metabolism. *Mol. Pharmacol. 89*, 435−445.
(25) Fang, X. J., Kobayashi, Y., and Halpert, J. R. (1997) Stoichiometry of 7-ethoxycoumarin metabolism by cytochrome P450 2B1 wild-type and five active-site mutants. *FEBS Lett. 416*, 77−80.
(26) Kobayashi, Y., Strobel, S. M., Hopkins, N. E., Alworth, W. L., and Halpert, J. R. (1998) Catalytic properties of an expressed cytochrome P450 2B1 from a Wistar-Kyoto rat liver cDNA library. *Drug Metab. Dispos. 26*, 1026−1030.
(27) Scott, E. E., White, M. A., He, Y. A., Johnson, E. F., Stout, C. D., and Halpert, J. R. (2004) Structure of mammalian cytochrome P450 2B4 complexed with 4-(4-chlorophenyl)imidazole at 1.9-Å resolution: Insight into the range of P450 conformations and the coordination of redox partner binding. *J. Biol. Chem. 279*, 27294−27301.
(28) Gay, S. C., Shah, M. B., Talakad, J. C., Maekawa, K., Roberts, A. G., Wilderman, P. R., Sun, L., Yang, J. Y., Huelga, S. C., Hong, W.-X., Zhang, Q., Stout, C. D., and Halpert, J. R. (2010) Crystal structure of a cytochrome P450 2B6 genetic variant in complex with the inhibitor 4-(4-chlorophenyl)imidazole at 2.0-Å resolution. *Mol. Pharmacol. 77*, 529−538.
(29) Talakad, J. C., Wilderman, P. R., Davydov, D. R., Kumar, S., and Halpert, J. R. (2010) Rational engineering of cytochromes P450 2B6 and 2B11 for enhanced stability: Insights into structural importance of residue 334. *Arch. Biochem. Biophys. 494*, 151−158.
(30) Wilderman, P. R., Gay, S. C., Jang, H. H., Zhang, Q., Stout, C. D., and Halpert, J. R. (2012) Investigation by site-directed mutagenesis of the role of cytochrome P450 2B4 non-active-site residues in protein-ligand interactions based on crystal structures of the ligand-bound enzyme. *FEBS J. 279*, 1607−1620.
(31) Strobel, S. M., and Halpert, J. R. (1997) Reassessment of cytochrome P450 2B2: catalytic specificity and identification of four active site residues. *Biochemistry 36*, 11697−11706.
(32) Szklarz, G. D., He, Y. Q., Kedzie, K. M., Halpert, J. R., and Burnett, V. L. (1996) Elucidation of amino acid residues critical for unique activities of rabbit cytochrome P450 2B5 using hybrid enzymes and reciprocal site-directed mutagenesis with rabbit cytochrome P450 2B4. *Arch. Biochem. Biophys. 327*, 308−318.
(33) He, Y., Luo, Z., Klekotka, P. A., Burnett, V. L., and Halpert, J. R. (1994) Structural determinants of cytochrome P450 2B1 specificity: evidence for five substrate recognition sites. *Biochemistry 33*, 4419−4424.
(34) He, Y. Q., Szklarz, G. D., and Halpert, J. R. (1996) Interconversion of the androstenedione hydroxylase specificities of cytochromes P450 2B4 and 2B5 upon simultaneous site-directed mutagenesis of four key substrate recognition residues. *Arch. Biochem. Biophys. 335*, 152−160.
(35) Kumar, S., Scott, E. E., Liu, H., and Halpert, J. R. (2003) A rational approach to re-engineer cytochrome P450 2B1 regioselectivity based on the crystal structure of cytochrome P450 2C5. *J. Biol. Chem. 278*, 17178−17184.
(36) Shah, M. B., Wilderman, P. R., Pascual, J., Zhang, Q. H., Stout, C. D., and Halpert, J. R. (2012) Conformational adaptation of human cytochrome P450 2B6 and rabbit cytochrome P450 2B4 revealed upon binding multiple amlodipine molecules. *Biochemistry 51*, 7225−7238.
(37) Omura, T., and Sato, R. (1964) Carbon monoxide-binding pigment of liver microsomes. I. Evidence for its hemoprotein nature. *J. Biol. Chem. 239*, 2370−2378.
(38) Omura, T., and Sato, R. (1964) Carbon monoxide-binding pigment of liver microsomes. II. Solubilization purification and properties. *J. Biol. Chem. 239*, 2379−2385.
(39) Kobayashi, Y., Fang, X., Szklarz, G. D., and Halpert, J. R. (1998) Probing the active site of cytochrome P450 2B1: metabolism of 7-alkoxycoumarins by the wild type and five site-directed mutants. *Biochemistry 37*, 6679−6688.
(40) Harlow, G. R., He, Y. A., and Halpert, J. R. (1997) Functional interaction between amino-acid residues 242 and 290 in cytochromes P-450 2B1 and 2B11. *Biochim. Biophys. Acta, Protein Struct. Mol. Enzymol. 1338*, 259−266.

DOI: 10.1021/acs.biochem.7b00097
Biochemistry 2017, 56, 2238−2246

(41) Holmans, P. L., Shet, M. S., Martin-Wixtrom, C. A., Fisher, C. W., and Estabrook, R. W. (1994) The high-level expression in *Escherichia coli* of the membrane-bound form of human and rat cytochrome b5 and studies on their mechanism of function. *Arch. Biochem. Biophys. 312*, 554−565.
(42) Paulsen, M. D., Bass, M. B., and Ornstein, R. L. (1991) Analysis of active site motions from a 175 ps molecular dynamics simulation of camphor-bound cytochrome P450cam. *J. Biomol. Struct. Dyn. 9*, 187−203.
(43) Paulsen, M. D., and Ornstein, R. L. (1992) Predicting the product specificity and coupling of cytochrome P450cam. *J. Comput.-Aided Mol. Des. 6*, 449−460.
(44) Szklarz, G. D., and Halpert, J. R. (1998) Molecular basis of P450 inhibition and activation. Implications for drug development and drug therapy. *Drug Metab. Dispos. 26*, 1179−1184.
(45) Szklarz, G. D., He, Y. A., and Halpert, J. R. (1995) Site-directed mutagenesis as a tool for molecular modeling of cytochrome P450 2B1. *Biochemistry 34*, 14312−14322.
(46) Szklarz, G. D., and Paulsen, M. D. (2002) Molecular modeling of cytochrome P450 1A1: enzyme-substrate interactions and substrate binding affinities. *J. Biomol. Struct. Dyn. 20*, 155−162.
(47) Kent, U. M., Hanna, I. H., Szklarz, G. D., Vaz, A. D. N., Halpert, J. R., Bend, J. R., and Hollenberg, P. F. (1997) Significance of glycine 478 in the metabolism of N-benzyl-1-aminobenzotriazole to reactive intermediates by cytochrome P450 2B1. *Biochemistry 36*, 11707−11716.
(48) Strobel, S. M., Szklarz, G. D., He, Y., Foroozesh, M., Alworth, W. L., Roberts, E. S., Hollenberg, P. F., and Halpert, J. R. (1999) Identification of selective mechanism-based inactivators of cytochromes P-450 2B4 and 2B5, and determination of the molecular basis for differential susceptibility. *J. Pharmacol. Exp. Ther. 290*, 445−451.
(49) Ericksen, S. S., and Szklarz, G. D. (2005) Regiospecificity of human cytochrome P450 1A1-mediated oxidations: the role of steric effects. *J. Biomol. Struct. Dyn. 23*, 243−256.
(50) Huang, Q., and Szklarz, G. D. (2010) Significant increase in phenacetin oxidation on L382V substitution in human cytochrome P450 1A2. *Drug Metab. Dispos. 38*, 1039−1045.
(51) Tu, Y., Deshmukh, R., Sivaneri, M., and Szklarz, G. D. (2008) Application of molecular modeling for prediction of substrate specificity in cytochrome P450 1A2 mutants. *Drug Metab. Dispos. 36*, 2371−2380.
(52) Walsh, A. A., Szklarz, G. D., and Scott, E. E. (2013) Human cytochrome P450 1A1 structure and utility in understanding drug and xenobiotic metabolism. *J. Biol. Chem. 288*, 12932−12943.
(53) Nebert, D. (1987) P450 Genes: Structure, Evolution, And Regulation. *Annu. Rev. Biochem. 56*, 945−993.
(54) Kumar, S., Chen, C. S., Waxman, D. J., and Halpert, J. R. (2005) Directed evolution of mammalian cytochrome P450 2B1: Mutations outside of the active site enhance the metabolism of several substrates, including the anticancer prodrugs cyclophosphamide and ifosfamide. *J. Biol. Chem. 280*, 19569−19575.
(55) Mo, S. L., Liu, Y. H., Duan, W., Wei, M. Q., Kanwar, J. R., and Zhou, S. F. (2009) Substrate specificity, regulation, and polymorphism of human cytochrome P450 2B6. *Curr. Drug Metab. 10*, 730−753.
(56) Zanger, U. M., and Klein, K. (2013) Pharmacogenetics of cytochrome P450 2B6 (CYP2B6): advances on polymorphisms, mechanisms, and clinical relevance. *Front. Genet. 4*, 24.
(57) Arteaga, S., Andrade-Cetto, A., and Cardenas, R. (2005) *Larrea tridentata* (Creosote bush), an abundant plant of Mexican and US-American deserts and its metabolite nordihydroguaiaretic acid. *J. Ethnopharmacol. 98*, 231−239.
(58) Mabry, T. J., DiFeo, D. R., Jr., Sakakibara, M., Bohnstedt, C. F., Jr., and Seigler, D. (1977) The natural products chemistry of *Larrea*. In *Creosote Bush: Biology and Chemistry of Larrea in New World Deserts* (Mabry, T. J., Hunzike, J., and DiFeo, D. R., Jr., Eds.) pp 115−134, Dowden, Hutchinson & Ross Inc., Stroudsburg, PA.

DOI: 10.1021/acs.biochem.7b00097
Biochemistry 2017, 56, 2238−2246